Advances in Geo-Energy Research

Vol. 11, No. 3, p. 230-240, 2024

Original article

Small angle neutron scattering studies of shale oil occurrence status at nanopores

Tao Zhang[1,2], Qinhong Hu[2,3]*, Qiang Tian[4], Yubin Ke[5,6], Qiming Wang[2]

[1]*Department of Earth and Environmental Sciences, University of Texas at Arlington, Arlington 76019, USA*

[2]*National Key Laboratory of Deep Oil and Gas, China University of Petroleum (East China), Qingdao 266580, P. R. China*

[3]*Laboratory for Marine Mineral Resource, Qingdao Marine Science and Technology Center, Qingdao 266071, P. R. China*

[4]*State Key Laboratory of Environment-Friendly Energy Materials, Southwest University of Science and Technology, Mianyang 621010, P. R. China*

[5]*Spallation Neutron Source Science Center, Dongguan 523803, P. R. China*

[6]*Institute of High Energy Physics, Chinese Academy of Sciences, Beijing 100049, P. R. China*

Keywords:
Small angle neutron scattering
organic shale
oil occurrence status
nano-sized pores
radius of gyration

Cited as:
Zhang, T., Hu, Q., Tian, Q., Ke, Y., Wang, Q. Small angle neutron scattering studies of shale oil occurrence status at nanopores. Advances in Geo-Energy Research, 2024, 11(3): 230-240. https://doi.org/10.46690/ager.2024.03.07

Abstract:
Utilizing small angle neutron scattering techniques on organic shales, this study presents an innovative approach for characterizing the status of oil occurrence, and new insights into pore scale assessment through scattering vector-pore size relationship. The results indicate the successful identification of different shale oil occurrence status, before and after solvent extraction of residual oil for four shale samples with different contents of total organic carbon. In addition, coupled with density distribution analyses, the work demonstrates that shale samples with lower total organic carbon contents typically signify a smaller radius of gyration with better oil mobility, which indicates a greater wave oscillation with a larger pore size to be estimated from the scattering vector. This work also elucidates the notable scenarios of an increasing pore size could correspond to a decreasing radius of gyration caused by mass density redistribution. For polydisperse systems, this research illustrates the variations in pore volumetric ratio impact the scattering intensity, whereas pore scale changes affect the oscillation pattern. This novel research of analyzing mass density distribution and pore scale information in real space is also suitable for other porous media systems.

1. Introduction

Shale, recognized as a typically polydisperse porous medium, garners a substantial attention owing to its complex geometric characteristics and vast utilities in geological systems such as being unconventional hydrocarbon reservoirs (Nelson, 2009; Ross and Bustin, 2009; Clarkson et al., 2012). The topics of ultra-low matrix permeability (Zhang et al., 2023), wide pore size distribution (PSD) (Sakurovs et al., 2012; Kuila and Prasad, 2013; Xu, 2020), complex oil occurrence status (Xu et al., 2022), and μm-scale mixed wettability (Hu et al., 2015) have emerged as crucial foci for an efficient development of shale oil, thereby receiving considerable studies. However, despite recent advancements (Wang et al., 2016; Hu et al., 2021; Li and Cai, 2023a), achieving direct nm-scale insights of oil occurrence status still remains challenging, resulting in a gap of a comprehensive understanding of shale oil mobility within pore spaces and subsequent production in wellbores (He et al., 2015; Saif et al., 2016).

Small angle neutron scattering (SANS) techniques serve as a unique technique for the structural characterization of geological media (Radliński et al., 1999, 2000; Clarkson et al., 2013; Anovitz and Cole, 2015; Zhang et al., 2020). Based on the way that neutrons interact and scatter from atoms, SANS provides the means to probe the atomic information

Yandy Scientific Press

*Corresponding author.
E-mail address: tao.1220@outlook.com (T. Zhang); huqinhong@upc.edu.cn (Q. Hu); tianqiang@swust.edu.cn (Q. Tian); keyb@ihep.ac.cn (Y. Ke); wqmpetrophysics@sina.com (Q. Wang).

Received February 4, 2024; revised February 26, 2024; accepted March 13, 2024; available online March 17, 2024.

Table 1. Sample properties and SLD values.

ID	TOC (wt.%)	R_o(%)	SLD ($\times 10^{10}$ cm^{-2})
C1	1.07	1.05±0.06	3.94
C2	1.67	1.06±0.07	4.04
C3	2.91	1.02±0.05	4.01
C4	3.98	1.03±0.06	4.11

Note: R_o is the % of reflected light at the specified wavelength from a vitrinite maceral immersed in oil for maturity indication. The average OM mass density and associated SLD value of 1.22 g/cm^3 and 3.5×10^{10} cm^{-2} were used for calculation.

and thereby provides an opportunity to assess the redistribution of mass during the new arrangement of components (Jeffries et al., 2020). The SANS method has been extensively employed in the realm of structured polymers and proteins (Cousin et al., 2005; Liu et al., 2009; Hong et al., 2012), e.g., in analyzing the conformational alterations when higher-order assemblies are forged of macromolecules (Arrighi et al., 2004). Despite its effectiveness in numerous fields, a comparable approach for analyzing mass distribution within shale oil formations is yet to be fully developed.

Meanwhile, the interpretation of SANS data, particularly in understanding pore-scale phenomena in geologic systems as inferred from scattering patterns, continues to be a subject of controversy (Gu et al., 2015; Guo et al., 2019; He et al., 2020). According to the reciprocity law (Glatter and Kratky, 1982; Iampietro et al., 1998), the characteristic size of an object, denoted as r, is inversely correlated with the width of scattering intensity distribution, $I(q)$, in q-space (Chen, 1986). Mathematically, in fact, the expression of scattering vector in neutron coherent elastic scattering is an alignment with Bragg scattering, to be the same as $q = 2\pi/d$ as illustrated by Squires (1996), which offers a way for scale assessment. This alignment, however, is contingent upon conditions and could fail in certain scenarios. For instance, when particle interference effects appear in densely-packed particles, the scattering pattern resembles what is expected from a distorted crystal lattices pattern on a large scale (Glatter and Kratky, 1982), like particles spanning a range of distances or be densely-compacted as in geologic systems. Consequently, by considering that only perfectly periodic distributions result in lattice peak functions in the Fourier transforms (Ewald, 1940), the straightforward application of $q = 2\pi/d$ faces challenges in estimating particulate scattering in non-periodic, distorted systems in real space. Even empirical values, e.g., $r = 2.5/q$, have been proposed for estimating the structural scale of geomedia (Radliński et al., 2000; Melnichenko et al., 2012), the q vs. r correlation still falls short in providing a well-justified quantification regarding the closely-packed polydisperse systems like shales.

In light of the complexities inherent in studying the oil occurrence status and structural scales in shale, this research is driven by three pivotal objectives:

1) This study evaluates the occurrence status of oil (whether being adsorbed or freely moving) within pore systems, leveraging mass density (from the scattering length density (SLD) of neutrons) spatial distribution (MSD) analyses in SANS;
2) The correlation between the scattering vector q and the pore radius r is explored in closely-packed geologic systems for a practical utilization of PSD characterization;
3) The potential relationship between MSD and particle scale in porous media is elucidated from SANS data before and after solvent extraction treatment of oil-producing shale samples.

2. Materials and methodologies

2.1 Samples and experiments

Four lacustrine-sourced shale core samples, collected from the Kongdian Formation in Cangdong Sag of the Bohai Bay Basin in China (Ma et al., 2021), in thin slab forms measuring between 500 and 800 μm in thickness were utilized. To examine the oil occurrence status and pore-scale characteristics, two distinct methodologies were employed. The first approach involved using natural samples with varying amounts of organic matter (OM), as indicated by total organic carbon (TOC) values ranging from 1 to 4 wt.% (Table 1). The second strategy employed "washing" treatment of oil-producing shale samples, with the objective of modifying the distribution of oil molecules in pore systems. These "washed" samples were treated with solvent extraction (SE) using solvents of dichloromethane (93%) and methanol (7%) (Table 1), and the SE was performed at 50 °C for seven days followed by oven-drying for 24 hrs at 60 °C. The underlying hypothesis is that natural samples with varying TOC contents, or washed samples by reagents, could result in a variation of MSD at different pore scales, based on previous investigations (Shawaqfeh and Al-Harahsheh, 2004; DiStefano et al., 2016).

The SANS experiments were conducted at Spallation Neutron Source (SNS) of Oak Ridge National Laboratory (ORNL) in the US, and at Chinese Spallation Neutron Source (CSNS) in China. The q-range for BL-6 Extended q-Range (EQ-SANS) Diffractometer at ORNL was from 0.00429 to 0.74 Å^{-1}, while the CSNS-SANS was from 0.0044 to 0.59 Å^{-1}. The USANS performed at ORNL have the probing q-range from 0.00001 to 0.00305 Å^{-1}. Since USANS usually take a longer measurement time (8-12 hrs) for each sample, only dry samples were analyzed by USANS in this study. Fig. 1 demonstrates the general information interpreted from USANS spectra for shale Sample C3.

2.2 Analyses of oil occurrence status

Shale pore structures are characterized by a notable heterogeneity and polydispersity, as illustrated in Figs. 2(a)-2(d). Significantly, oil molecules have a strong association with the pore spaces related to organic matter in organic shale. This association is underscored by statistical data of 3D images obtained by focused ion beam-scanning electron microscopy, which indicates that almost all these observed pores of >20 nm in diameters is adjacent to OM through

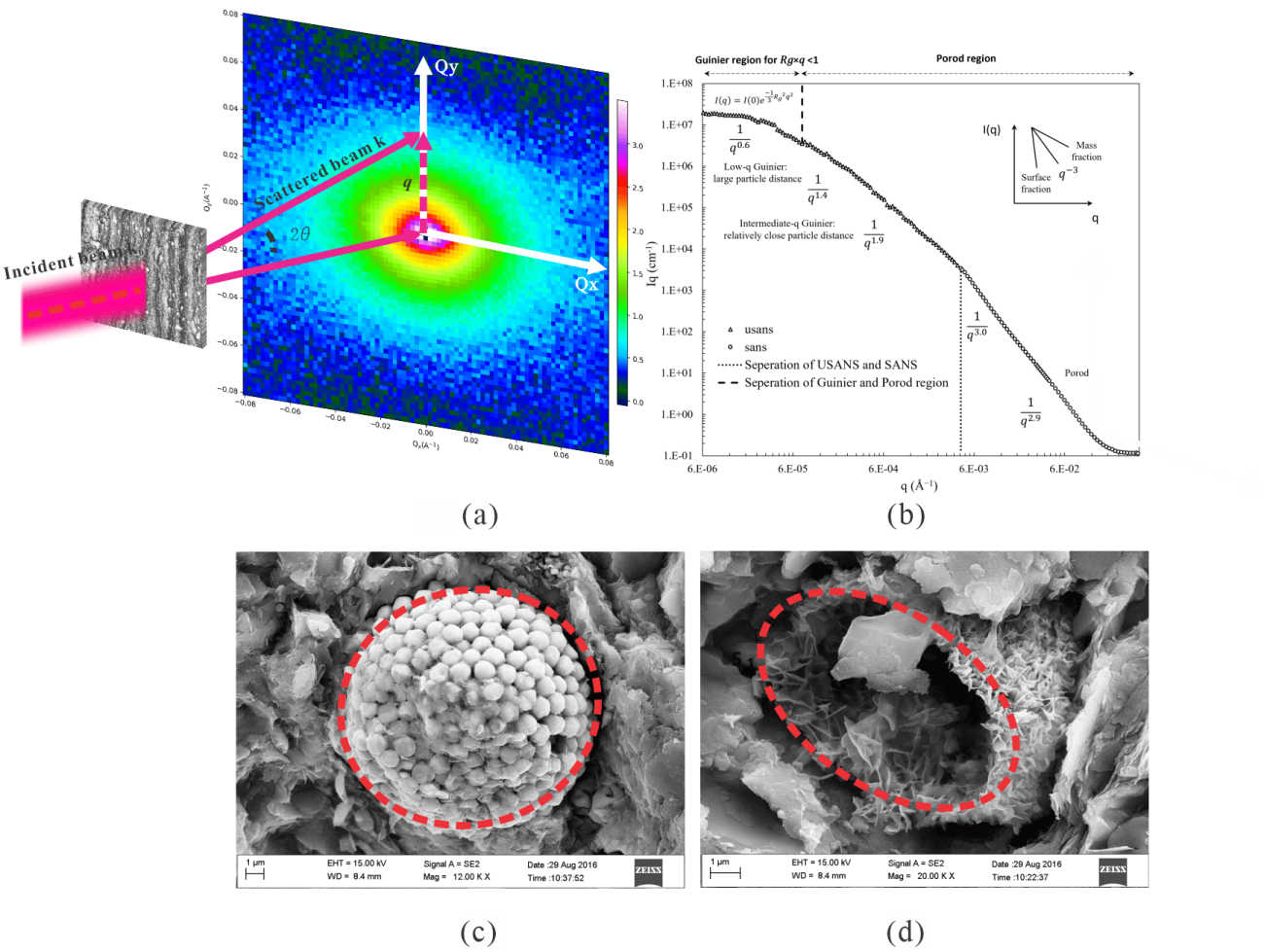

Fig. 1. General data information interpreted from USANS spectra for shale Sample C3. (a) The term 2θ denotes the angle between the incident and scattered neutron vectors; (b) vector $k = 2\pi/\lambda$ and $q = 4\pi \sin\theta/\lambda$. Here, λ is the wavelength. By incorporating q into Bragg's law of $\lambda = 2d \sin\theta$, we obtain the relation of $d = 2\pi/q$ to estimate ordered lattice spacings. The combined USANS and SANS scattering in the Guinier and Porod regions reveals a mass fractal behavior with values ranging from 2.9 to 3.0. (c-d) Additionally, typical shale structures, highlighting the varying scales of neutron interaction potential, from chaotic nanometer-sized pores to micrometer-sized components, are showcased.

3D digital rock analyses (Fig. 2(c)). A possible explanation for this phenomenon is the oil micro-migration from areas rich in organic materials to neighboring regions with poor TOC contents, and such a micro-migration has a considerable impact on both the distribution and composition of shale oil, as indicated by Li and Cai (2023a) and Hu et al. (2024). Within these spaces, oil molecules, described as dense, highly viscous, chemically intricate liquid hydrocarbons with a high carbon-to-hydrogen ratio (He et al., 2015; Bai et al., 2023), could predominantly exist in both free and adsorbed states (Zhang et al., 2019; Li et al., 2021, 2023b; Xu et al., 2022). Meanwhile, liquid hydrocarbons could co-exist with molecular gases and water (Li et al., 2023c).

The radius of gyration, R_g, represents the root-mean-square distance of all nuclei from their centers of gravity. It is typically determined through three distinct methods: the Guinier approximation (Guinier et al., 1955), analysis of the distance distribution function via indirect Fourier Transformation, and evaluation based on the position of the first subsidiary maximum in the scattering curve, the latter of which is only suitable for particles uniform in both composition and shape (Glatter and Kratky, 1982). These methods facilitate the characterization of the spatial distribution of mass within a particle. In the context of assessing the occurrence status of oil-dominated matter subjected to SE processes, the patterns of MSD are investigated using the radius of gyration, R_g. This approach is pivotal in quantifying how the particle's mass is distributed relative to its center of mass, as detailed by Celotta and Levine (1986):

$$R_g^2 = \frac{\Sigma_i b_i (r_i - r_c)^2}{\Sigma_i b_i} \tag{1}$$

Eq. (1) encompasses two key aspects: the size being defined by the relative distance between any atom r_i and the central atom r_c, and MSD patterns arising from the scattering length of b_i. When every atom within the particle is distributed

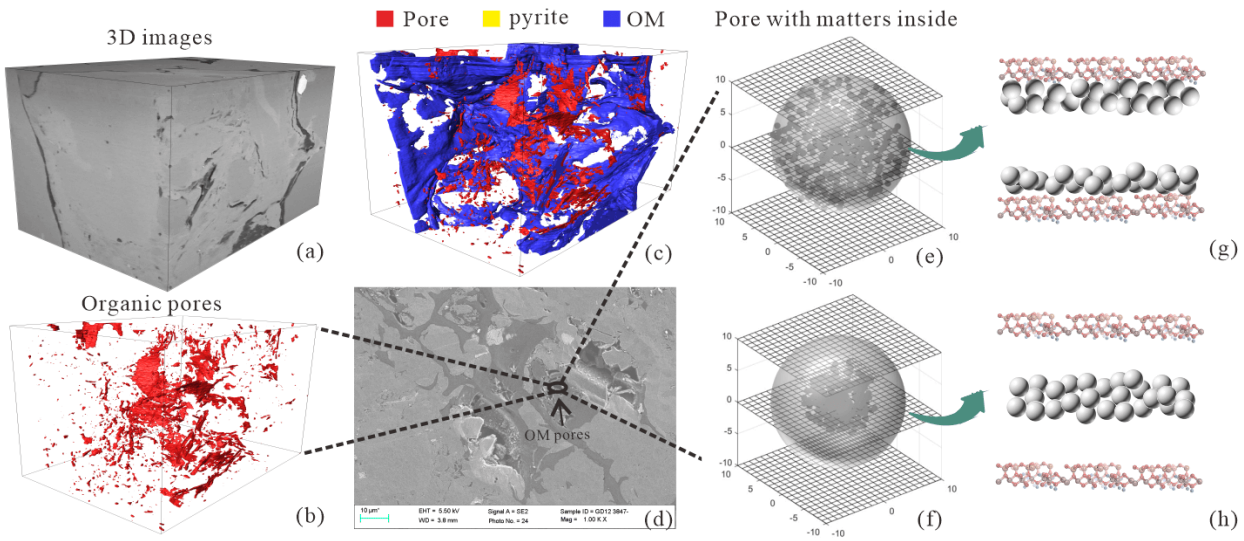

Fig. 2. Schematic of MSD patterns and oil occurrence status. (a)-(c) Pore morphology from three dimensional focused ion beam-scanning electron microscopy image stacks and (d) 2D SEM images of shale Sample C3. In image (c), colors of red, blue, and yellow represent pore space, organic matter, and pyrite, respectively. (e)-(f) demonstrate two different R_g status, (g) depicts oil absorption on the surface of pores and (h) illustrates a condition where the oil is in a more freely moving state.

on the surface and maintains a distance from the center of mass at atom r_c (Fig. 2(e)), R_g equals r. This situation suggests that oil molecules exist in an adsorbed state, adhering to the surface area, as illustrated in Fig. 2(g). Conversely, when $R_g = 0$, as deduced from $(r_i - r_c)^2 = 0$, it implies that all atoms r_i are aggregated at the mass center, coinciding with atom r_c (Fig. 2(f)). This scenario indicates that most oil molecules are situated at the center of pores, with probably free-moving state for an enhanced oil mobility, as depicted in Fig. 2(h). Building on this foundation, the mass density distribution of oil molecules in relation to their occurrence status is analyzed in Section 3-2 via the average R_g value from the samples.

3. Data analyses and discussion

3.1 Variations of MSD with TOC contents

By virtue of the radius of gyration analyses, two key phenomena (Fig. 3) are observed. Firstly, natural shale samples with varying TOC contents exhibit an inherent heterogeneity in MSD properties. Specifically, Fig. 3(a) shows that R_g follows the same trend as the TOC values for both dry and SE samples, which indicates that with different TOC contents present in the sample, the oil molecules are distributed in different fashion. Secondly, the "washing" treatment has altered the MSD of samples, as evidenced by the decrease in R_g when compared to the dry samples in Fig. 3(a). This implies an enhanced oil mobility after the "washing" process, and the original oil molecules predominantly exist in a more adsorbed state on the pore surface of dry samples, corresponding to the situation of Fig. 2(e). In conjunction with Fig. 3(b), TOC contents are observed to be inversely proportional to clay values. Therefore, this research concludes that the natural abundance of OM can lead to uneven mass distribution in pore spaces, and a lower TOC content, typically correlating with a lower radius of gyration and higher clays contents, usually indicates better mobility of oil molecules in shales.

3.2 Correlation between pore scales and scattering vectors

In polydisperse systems, Guinier's approximation allows for structural analysis of widely spaced particles by ignoring interparticle interactions (Guinier, 1939). In this case, the scattering intensity follows an exponential decay with a slope of $-(qR_g)^2/3$, which provides a scale estimation at low q values where $qR_g < 1$ (Hammouda, 2012). However, this approximation breaks down in densely packed systems, where the total scattering cannot be simplistically construed as a mere summation of single-particle intensities due to the significant interparticle interference. In such scenarios, drawing insights from seminal works (Zernike and Prins, 1927; Fournet, 1951a, 1951b, 1951c; Guinier et al., 1955), when accounting for spherically symmetric particle with multiple types and varying sizes, one can derive the scattering intensity formula for ensembled particles with different types as:

$$I(q) = \sum_k p_k \overline{F_k^2(q)} + \frac{(2\pi)^{\frac{3}{2}}}{v_a} \sum_k \sum_j p_k p_j \overline{F_k(q)}\,\overline{F_j(q)} \left[g_{kj}(q) + \varepsilon_{kj}\beta_{kj}(q)\right] \quad (2)$$

The detailed step-by-step formulations are presented in Supplementary file. Eq. (2) is derived by considering the average orientations and positions of particles within the system. The first sum term in this equation provides insights into the size and shape of each particle type, as represented by the form factor $F_k(q)$. The second term, a double sum, accounts for the interference effects arising from the relative

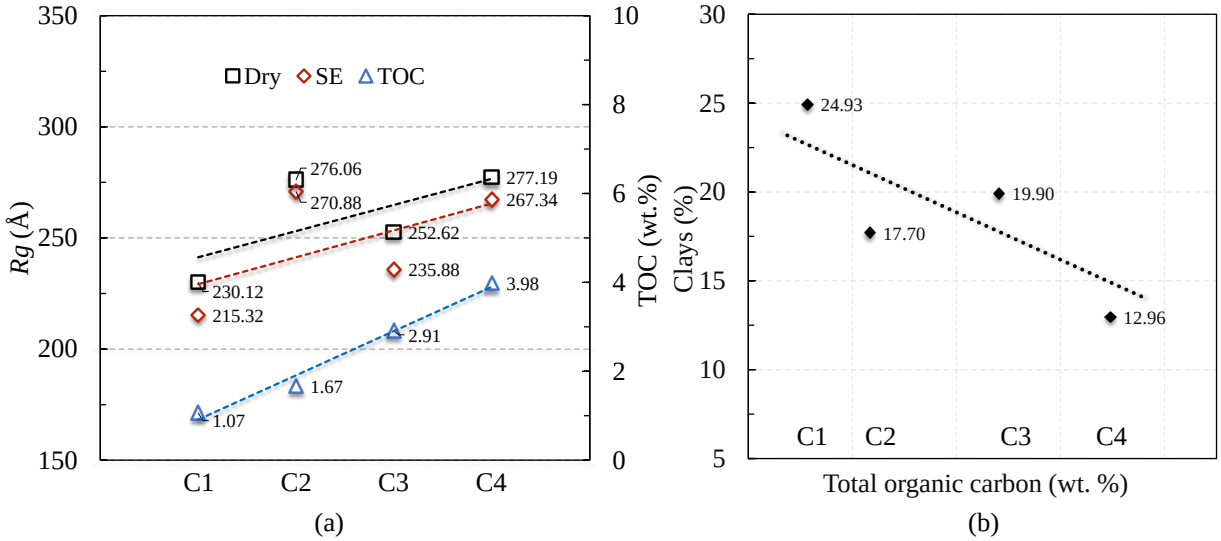

Fig. 3. (a) R_g for dry and "washed" samples; (b) correlation between TOC with clays. The dashed line indicates a trend in both (a) and (b). Notably, the deviation of the data, especially for Sample C2 in (a), could also be influenced by its largest depth of four samples, as Samples C1-C4 were collected from depths of 3,825, 4,093, 2,964, and 4,048 meters below the ground, respectively.

positions of particle pairs. In this context, p denotes the probability associated with a specific particle type, while v_a represents the average volume of all particles. Meanwhile, the functions $g_{kj}(q)$ and $\beta_{kj}(q)$ are introduced to describe the spatial distribution and interactions between particles of types k and j, respectively. The coefficient ε_{kj} modulates the interaction term. To accurately depict the variation in particle density with distance r from a reference particle, the radial distribution function $P_{kj}(r)$ (Yuste and Santos, 1991) is employed as:

$$P_{kj}(r) = \mathrm{e}^{-\frac{v_{kj}(r)}{kT}+f_{kj}(r)} \tag{3}$$

$P_{kj}(r)$ is expressed as a combined function of $g_{kj}(q)$ and $\beta_{kj}(q)$ in Eq. (S12) in Supplementary file, where $v_{kj}(r)$ represents the pairwise potential between particles, while k and T are the Boltzmann constant and temperature. The function $f_{kj}(r)$ is introduced to further refine the radial distribution function, capturing additional correlations beyond simple pairwise interactions. The formulation begins with gas-like systems as a starting point. Considering hard spheres where the potential $v_{kj}(r)$ becomes infinite for $r < 2R$, for the purposes of this analysis, ε_{kj} is assumed to equal 1, and $g_{kj}(q)$ is set to 0.

From the work of Rayleigh (1914), the form factor in Eq. (S14) of Supplementary file is transformed into the spherical Bessel function of the first kind, as outlined of Eq. (S15). Consequently, the independent variable in Eq. (S14) shifts to qr, with qr being designated as α.

Notably, though every particle scatters across all q vectors, each particle size contributes to the intensity in a unique manner with specific scales playing a more dominant role (Brumberger, 2013), as $I(q)$ is proportional to the square of sphere's volume with an order of r^6.

This work thereby investigates the system composed of two types of particles (R_1 and R_2), as being simulated in the Fig. 4. Figs. 4(a) and 4(b) simulate scenarios by adjusting the volumetric ratio from 10% to 90% while maintaining constant particle sizes at 10 and 20 Å. Conversely, Figs. 4(c)-4(f) depict systems with a fixed volumetric ratio of 50%, but with changing particle sizes. Specifically, in Figs. 4(c) and 4(d), R_1 varies from 10 to 28 Å while R_2 is constant at 20 Å; in Figs. 4(e) and 4(f), R_2 changes from 10 to 28 Å and R_1 remains at 10 Å. Notably, α is derived from the smaller one of two particle sizes in each scenario. From the analyses, Fig. 4 presents a conclusion that while the particle volumetric ratio has no impact on the intensity wave period of oscillation, variations in particle size significantly influence it. This is evident from the intensity extremum being observed at each α value. As shown in Figs. 4(a) and 4(b), changes in particle volume ratio did not alter the oscillation peak at a specific α. However, when the radius changes, a noticeable extreme shift appears at different α values no matter which particle is chosen for a size adjustment of R_1 and R_2, as being demonstrated in Figs. 4(c)-4(f).

3.3 Correlation between particle scale and density distribution

Since the α pattern indicates a changing correlation regarding the particle size r in real space and q in reciprocal space, and a correlation between them can be revealed to enable a pore size assessment in rock systems. This work thereby employs this correlation for PSD analyses which is critical for geo-media characterization (Melnichenko et al., 2012; Clarkson et al., 2013; Ruppert et al., 2013; Blach et al., 2020). In this work, the maximum-entropy method from Jemian et al. (1991) and the Irena package published by Ilavsky and

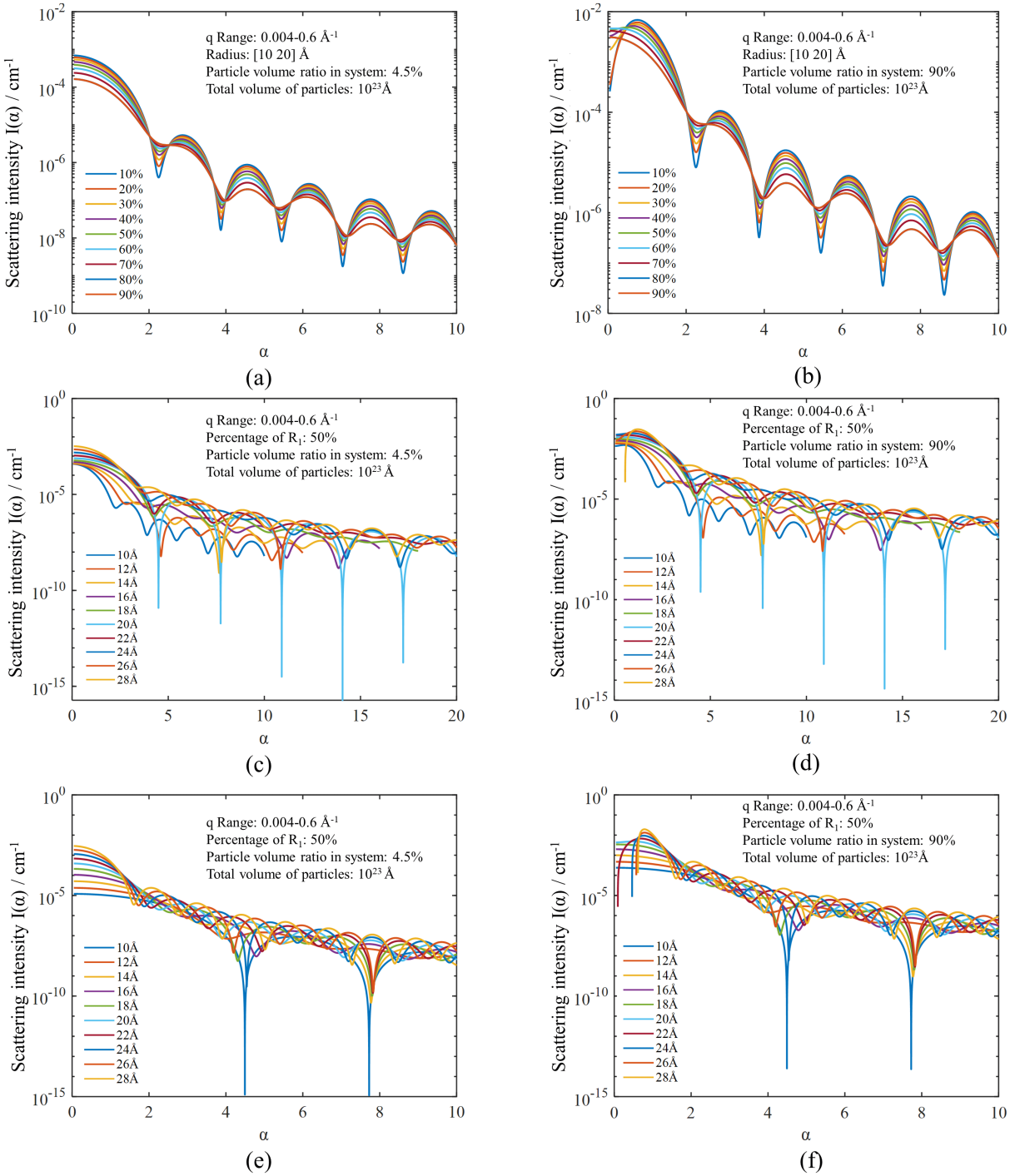

Fig. 4. Scattering intensities with variable α values. Panels (a), (c) and (e) depict systems with low percentage of porosity (4.5%) in solid porous media, while Panels (b), (d), and (f) showcase systems with high percentage (90% of liquids such as with colloids or proteins, or 90% of air mixed with solid particles). Therefore, this simulation is applicable to both high and low concentration systems (liquid or gas) when considering particle interactions, as they exhibit similar behaviors, differing only in intensity levels. In all scenarios, the total particle volume v_p is maintained as a constant 10^{23}, with a scattering vector q ranging from 0.004 to 0.6 Å. Notably, the simulated cohesive interactions (Tian et al., 2021) at low α region will not appear in shale systems owning to a complex pore structure.

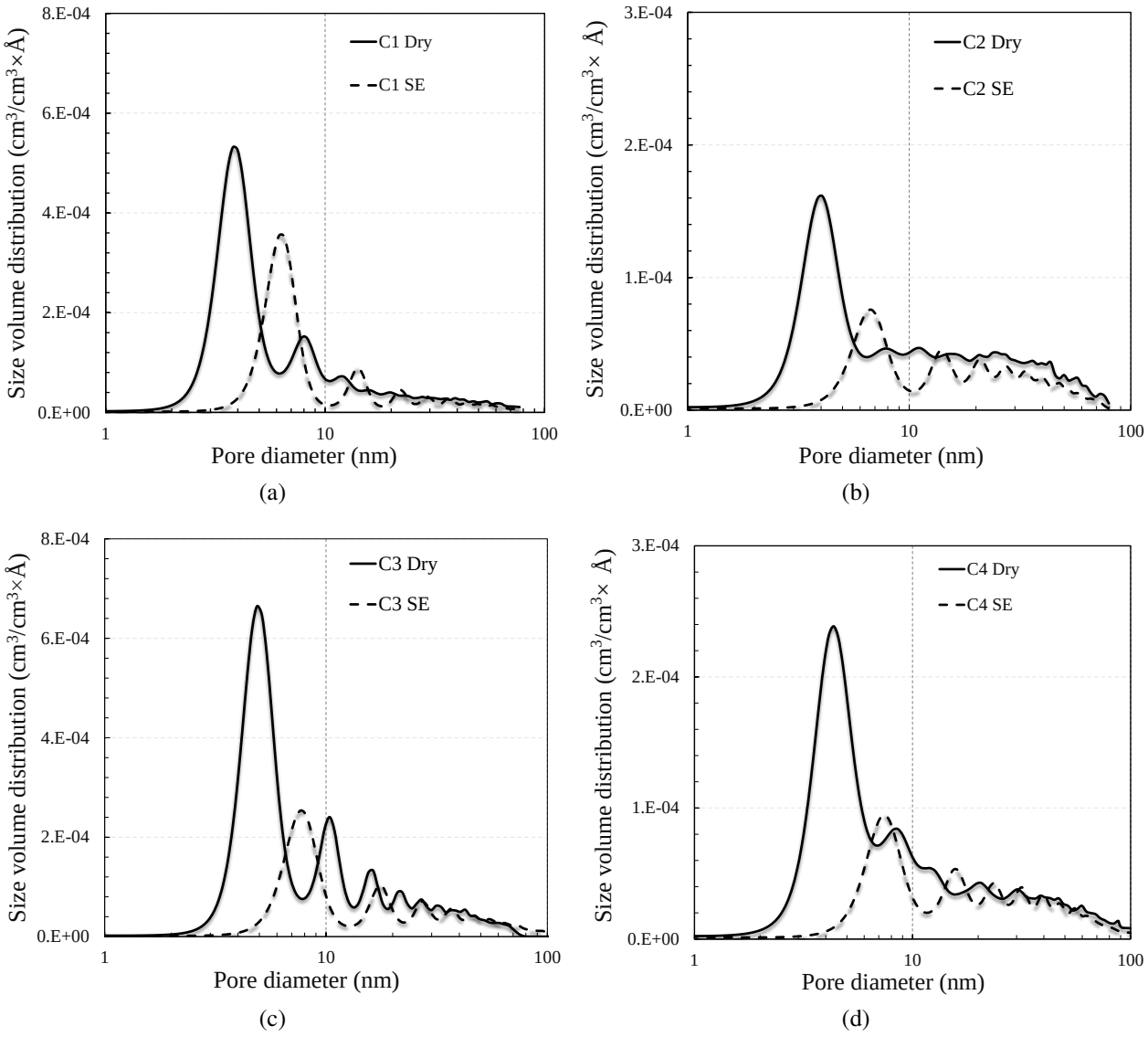

Fig. 5. PSD curve of the dry and "washed" samples, with (a), (b), (c) and (d) demonstrates the PSD curve for samples C1, C2, C3, and C4. On the Y-axis, the size volume distribution (per cm^3) represents the product of particle number and size, with a greater emphasis on particle number; the prominent peak in the left area of dashed vertical line thus does not mean a high percentage of porosity.

Jemian (2009) were employed for PSD and R_g interpretation, as illustrated in Fig. 5. Notably, α of 2.5 is adopted for a scale estimation for hollow polydisperse spheres from simulation as referenced in Radliński et al. (2000) with a justification by Melnichenko et al. (2012), which could be determined experimentally.

This work presents us with two significant conclusions. Firstly, the PSD curve distinctly reveals both pore scale and scattering intensity decrease for samples after "washing". As discussed previously, alterations in volumetric ratio result in intensity reductions at each extremum, while leaving the oscillation pattern (pore scale) unaffected, as exemplified in Figs. 4(a) and 4(b). However, a significant right-ward shift in the intensity peaks is evident in the PSD curve for the "washed" samples (Fig. 5), indicating an increase in pore sizes post-washing, rather than a mere decrease in intensity. This observation aligns with the phenomena illustrated in Figs. 4(c)-4(f), where wave oscillation shifts, induced by variations in pore size. In summary, the "washing" treatment induced the alteration of the pore spaces, corresponding to an increased pore radius r regarding the "washed" samples (Fig. 5).

Secondly, an increase in pore scale does not necessarily accompany the rise in R_g when the MSD variation simultaneously occurs in the system. Specifically, as discussed in Section 3-2 and evidenced in Fig. 5, a notable case was observed where the pore scale r increases, however, this coincides with a decrease in R_g in samples subjected to "washing". This phenomenon is explained in Fig. 6. Fig. 6(a) shows the dry samples characterized by a pore scale of R_a with most oil molecules concentrated between r_{ai} to r_c. Through "washing",

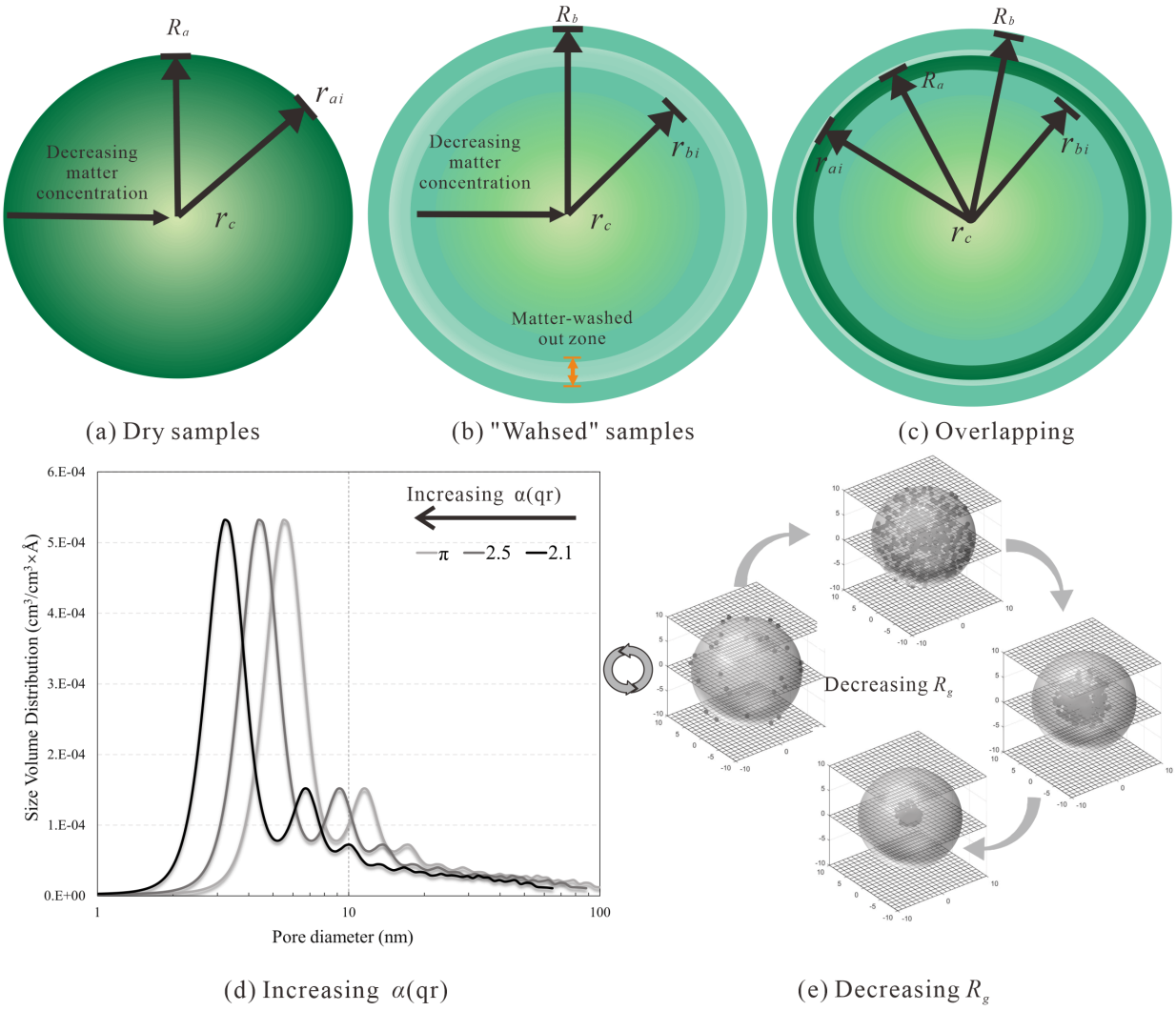

Fig. 6. Particle MSD and size information (a-c), and correlation between parameter α (d) and R_g status (e).

molecules near the inner surface of pores are dissolved and extracted, leading to an expanded pore size from R_a to R_b in Fig. 6(b), meanwhile, the "washing" process results in a decreased concentration of MSD in the "Matter washed-out zone" to be concentrated from r_{bi} to r_c (Fig. 6(b)). Consequently, the overlapping Fig. 6(a) and 6(b) is demonstrated in Fig. 6(c), which illustrates that despite an enlarged pore scale ($R_b > R_a$) being observed, the redistribution of matter results in a reduced ($r_{bi} < r_{ai}$) after "washing" treatment.

In summary, organic matter in the process of natural hydrocarbon generation exhibits inherent heterogeneity in shale, and the MSD analyses of unique SANS data is particularly relevant for shale systems due to the secondary migration of organic molecules from organic pores to mineral spaces. Thus, from with combined Fig. 6(d) and 6(e), this work further concludes that the integration of R_g behavior (Fig. 3) and size data (Fig. 5) from post-washing samples reveals a following key finding: A longer wave oscillation cycle, marked by larger values of α and pore size r (Fig. 6(d)), correlates with an increased mobility within pore spaces, as evidenced by the decreasing R_g value (Fig. 6(e)). Moreover, without consideration of mass density distribution of oil molecules, the radius of gyration may provide an opposite result regarding the size of pores. The correlation in Figs. 6(d) and 6(e) provides valuable insights into the dynamic structural and MSD evolution of geological materials.

4. Conclusions

By leveraging unique SANS techniques, this research elucidates the novel methodologies for characterizing MSD and extracting structural-scale information from reciprocal space in polydisperse porous media of organic shale. Specifically, the occurrence status of shale oil, whether being adsorbed onto pore surfaces or in a freely moving state, is illustrated through radius of gyration analyses of SANS data. Meanwhile, this study analyzed the distinct roles that particle size and volume ratio play in the $I(\alpha)$ vs. α ($\alpha = qr$) correlation. This analysis was conducted using an ensemble of particles of various types, employing the spherical Bessel function of the first kind, which was further utilized for PSD analyses to examine its correlation with MSD.

In conjunction with well-designed experiments and SANS

analyses, these theoretical methodologies lead to three key conclusions. Firstly, a lower TOC content typically correlates with a smaller radius of gyration, suggesting an improved mobility of oil molecules in shales. Secondly, in particle systems with a constant number, variations in volumetric ratio affect scattering intensity, while size changes influence the oscillation pattern. On this basis, organic shale with enhanced oil mobility within pore spaces will correspond to a larger α ($r = \alpha/q$) value, corresponding to a greater wave oscillation, indicates a more concentrated mass density distribution. Thirdly and most importantly, an increase in R_g does not always correspond to an enlargement in pore scale when the MSD is altered, as observed in this study. Additionally, the analysis of geometric information through scattering intensity is concurrently influenced by the distribution of mass density.

Acknowledgements

We acknowledge the funding support from the National Natural Science Foundation of China (No. 41821002), the PetroChina International Cooperation Project (No. 2023DQ0422), the Maverick Science Graduate Research Fellowship and Dissertation Fellowship at the University of Texas at Arlington, and the AAPG Foundation's Grants-in-Aid. For this work, SANS data have been collected from various beamlines via user proposals at international facilities of the CSNS and the SNS, a Department of Energy Office of Science User Facility operated by the ORNL. We especially appreciate the help from Drs. Wei-Ren Chen and Gergely Nagy at ORNL for the (U)SANS experiments and fruitful discussion. We would like to express our sincere gratitude to Editor Dr. J. Cai and three anonymous reviewers for their insightful suggestions that have significantly improved the quality of this paper.

Supplementary file

https://doi.org/10.46690/ager.2024.03.07

Conflict of interest

The authors declare no competing interest.

References

Anovitz, L. M., Cole, D. R. Characterization and analysis of porosity and pore structures. Reviews in Mineralogy and Geochemistry, 2015, 80(1): 61-164.

Arrighi, V., Gagliardi, S., Dagger, A. C., et al. Conformation of cyclics and linear chain polymers in bulk by SANS. Macromolecules, 2004, 37(21): 8057-8065.

Bai, L., Liu, B., Fu, X., et al. A new method for evaluating the oil mobility based on the relationship between pore structure and state of oil. Geoscience Frontiers, 2023, 14(6): 101684.

Blach, T., Radlinski, A. P., Edwards, D. S., et al. Pore anisotropy in unconventional hydrocarbon source rocks: A small-angle neutron scattering (SANS) study on the Arthur Creek Formation, Georgina Basin, Australia. International Journal of Coal Geology, 2020, 225: 103495.

Brumberger, H. Modern Aspects of Small-Angle Scattering. New York, USA, Springer Science & Business Media, 2013.

Celotta, R., Levine, J. Methods of Experimental Physics: Neutron Scattering Part A. Orlando, USA, Academic Press, 1986.

Chen, S. H. Small angle neutron scattering studies of the structure and interaction in micellar and microemulsion systems. Annual Review of Physical Chemistry, 1986, 37(1): 351-399.

Clarkson, C. R., Jensen, J. L., Chipperfield, S. Unconventional gas reservoir evaluation: What do we have to consider? Journal of Natural Gas Science and Engineering, 2012, 8: 9-33.

Clarkson, C. R., Solano, N., Bustin, R. M., et al. Pore structure characterization of North American shale gas reservoirs using USANS/SANS, gas adsorption, and mercury intrusion. Fuel, 2013, 103: 606-616.

Cousin, F., Gummel, J., Ung, D., et al. Polyelectrolyte-protein complexes: Structure and conformation of each specie revealed by SANS. Langmuir, 2005, 21(21): 9675-9688.

DiStefano, V. H., McFarlane, J., Anovitz, L. M., et al. Extraction of organic compounds from representative shales and the effect on porosity. Journal of Natural Gas Science and Engineering, 2016, 35: 646-660.

Ewald, P. P. X-ray diffraction by finite and imperfect crystal lattices. Proceedings of the Physical Society, 1940, 52(1): 167-174.

Fournet, G. Diffusion des rayons X par les fluides. Acta Crystallographica, 1951a, 4(4): 293-301. (in French)

Fournet, G. Étude théorique et expérimentale de la diffusion des rayons X par les ensembles denses de particules. Bulletin de Minéralogie, 1951b, 74(1): 37-172. (in French)

Fournet, G. Généralisation de la théorie cinétique des fluides de Born et Green aux ensembles de particules de plusieurs espèces différentes. Journal de Physique et Le Radium, 1951c, 12(5): 592-595. (in French)

Glatter, O., Kratky, O. Small Angle X-Ray Scattering. London, UK, Academic Press, 1982. (in French)

Gu, X., Cole, D. R., Rother, G., et al. Pores in Marcellus Shale: A Neutron Scattering and FIB-SEM Study. Energy & Fuels, 2015, 29(3): 1295-1308.

Guinier, A. La diffraction des rayons X aux très petits angles: Application à l'étude de phénomènes ultramicroscopiques. Annales de Physique, 1939, 11(12): 161-237. (in French)

Guinier, A., Fournet, G., Walker, C. B., et al. Small-angle Scattering of X-rays. New York, USA, John Wiley and Sons Inc, 1955.

Guo, X., Qin, Z., Yang, R., et al. Comparison of pore systems of clay-rich and silica-rich gas shales in the lower Silurian Longmaxi formation from the Jiaoshiba area in the eastern Sichuan Basin, China. Marine and Petroleum Geology, 2019, 101: 265-280.

Hammouda, B. Probing Nanoscale Structures-The SANS Toolbox, Gaithersburg, USA, 2012.

He, C., He, S., Zhang, T., Yang, R., Shu, Z., Han, Y. Structural characteristics and porosity estimation of organic matter-hosted pores in gas shales of Jiaoshiba Block, Sichuan Basin, China. Energy Science & Engineering, 2020, 8(12): 4178-4195.

He, L., Lin, F., Li, X., et al. Interfacial sciences in unconventional petroleum production: From fundamentals to applications. Chemical Society Reviews, 2015, 44(15): 5446-5494.

Hong, K., Liu, Y., Porcar, L., et al. Structural response of polyelectrolyte dendrimer towards molecular protonation: The inconsistency revealed by SANS and NMR. Journal of Physics: Condensed Matter, 2012, 24(6): 064116.

Hu, Q., Ewing, R. P., Rowe, H. D. Low nanopore connectivity limits gas production in Barnett formation. Journal of Geophysical Research: Solid Earth, 2015, 120(12): 8073-8087.

Hu, T., Jiang, F., Pang, X., et al. Identification and evaluation of shale oil micro-migration and its petroleum geological significance. Petroleum Exploration and Development, 2024, 51(1): 127-140.

Hu, T., Pang, X., Jiang, F., et al. Movable oil content evaluation of lacustrine organic-rich shales: Methods and a novel quantitative evaluation model. Earth-Science Reviews, 2021, 214: 103545.

Iampietro, D. J., Brasher, L. L., Kaler, E. W., et al. Direct analysis of SANS and SAXS measurements of catanionic surfactant mixtures by Fourier transformation. The Journal of Physical Chemistry B, 1998, 102(17): 3105-3113.

Ilavsky, J., Jemian, P. R. Irena: Tool suite for modeling and analysis of small-angle scattering. Journal of Applied Crystallography, 2009, 42(2): 347-353.

Jeffries, C. M., Pietras, Z., Svergun, D. I. The basics of small-angle neutron scattering (SANS for new users of structural biology). EPJ Web of Conferences, 2020, 236: 03001.

Jemian, P. R., Weertman, J. R., Long, G. G., et al. Characterization of 9Cr-1MoVNb steel by anomalous small-angle X-ray scattering. Acta Metallurgica et Materialia, 1991, 39(11): 2477-2487.

Kuila, U., Prasad, M. Specific surface area and pore size distribution in clays and shales. Geophysical Prospecting, 2013, 61: 341-362.

Li, J., Cai, J. Quantitative characterization of fluid occurrence in shale reservoirs. Advances in Geo-Energy Research, 2023a, 9(3): 146-151.

Li, R., Chen, Z., Wu, K., et al. An analytical model for water-oil two-phase flow in inorganic nanopores in shale oil reservoirs. Petroleum Science, 2021, 18(6): 1776-1787.

Li, S., Guo, Q., Pan, S., et al. Influence of intrasource micro-migration of hydrocarbons on the differential enrichment of laminated type shale oil: A case study of the third submember of the seventh member of the Triassic Yanchang Formation in Ordos Basin. China Petroleum Exploration, 2023b, 28(4): 46-54. (in Chinese)

Li, Z., Lei, Z., Shen, W., et al. A comprehensive review of the oil flow mechanism and numerical simulations in shale oil reservoirs. Energies, 2023c, 16(8): 3516.

Liu, Y., Bryantsev, V. S., Diallo, M. S., et al. PAMAM dendrimers undergo pH responsive conformational changes without swelling. Journal of the American Chemical Society, 2009, 131(8): 2798-2799.

Ma, B., Hu, Q., Yang, S., et al. Pore structure typing and fractal characteristics of lacustrine shale from Kongdian Formation in East China. Journal of Natural Gas Science and Engineering, 2021, 85: 103709.

Melnichenko, Y. B., He, L., Sakurovs, R., et al. Accessibility of pores in coal to methane and carbon dioxide. Fuel, 2012, 91(1): 200-208.

Nelson, P. H. Pore-throat sizes in sandstones, tight sandstones, and shales. AAPG Bulletin, 2009, 93(3): 329-340.

Radliński, A. P., Boreham, C. J., Lindner, P., et al. Small angle neutron scattering signature of oil generation in artificially and naturally matured hydrocarbon source rocks. Organic Geochemistry, 2000, 31(1): 1-14.

Radliński, A. P., Radlińska, E. Z., Agamalian, M., et al. Fractal geometry of rocks. Physical Review Letters, 1999, 82(15): 3078.

Rayleigh, L. On the diffraction of light by spheres of small relative index. Proceedings of the Royal Society of London. Series A, Containing Papers of a Mathematical and Physical Character, 1914, 90(617): 219-225.

Ross, D. J., Bustin, R. M. The importance of shale composition and pore structure upon gas storage potential of shale gas reservoirs. Marine and Petroleum Geology, 2009, 26(6): 916-927.

Ruppert, L. F., Sakurovs, R., Blach, T. P., et al. A USANS/SANS study of the accessibility of pores in the Barnett Shale to methane and water. Energy & Fuels, 2013, 27(2): 772-779.

Saif, T., Lin, Q., Singh, K., et al. Dynamic imaging of oil shale pyrolysis using synchrotron X-ray microtomography. Geophysical Research Letters, 2016, 43(13): 6799-6807.

Sakurovs, R., He, L., Melnichenko, Y. B., et al. Pore size distribution and accessible pore size distribution in bituminous coals. International Journal of Coal Geology, 2012, 100: 51-64.

Shawaqfeh, A., Al-Harahsheh, A. Solvation of Jordanian oil shale using different organic solvents by continuous contact mixing. Energy Sources, 2004, 26(14): 1321-1330.

Squires, G. L. Introduction to the Theory of Thermal Neutron Scattering. Cambridge, UK, Courier Corporation, 1996.

Tian, Q., Sun, J., Henderson, M. J., et al. Quantitative analysis of the structural relaxation of silica-PEO shake gel by X-ray and light scattering. Polymer Testing, 2021, 104: 107391.

Wang, S., Javadpour, F., Feng, Q. Molecular dynamics simulations of oil transport through inorganic nanopores in shale. Fuel, 2016, 171: 74-86.

Xu, H. Probing nanopore structure and confined fluid behavior in shale matrix: A review on small-angle neutron scattering studies. International Journal of Coal Geology, 2020, 217: 103325.

Xu, Y., Lun, Z., Pan, Z., et al. Occurrence space and state of shale oil: A review. Journal of Petroleum Science and

Engineering, 2022, 211: 110183.

Yuste, S. B., Santos, A. Radial distribution function for hard spheres. Physical Review A, 1991, 43(10): 5418.

Zernike, F., Prins, J. A. Die Beugung von Röntgenstrahlen in Flüssigkeiten als Effekt der Molekülanordnung. Zeitschrift für Physik A Hadrons and Nuclei, 1927, 41(2): 184-194. (in French)

Zhang, T., Hu, Q., Ghanbarian, B., et al. A pulse-decay method for low (matrix) permeability analyses of granular rock media. Hydrology and Earth System Sciences, 2023, 27(24): 4453-4465.

Zhang, W., Feng, Q., Wang, S., et al. Oil diffusion in shale nanopores: Insight of molecular dynamics simulation. Journal of Molecular Liquids, 2019, 290: 111183.

Zhang, Y., Hu, Q., Barber, T. J., et al. Quantifying fluid-wettable effective pore space in the Utica and Bakken oil shale formations. Geophysical Research Letters, 2020, 47(14): e2020GL087896.